J. Fluid Mech. (2013), *vol.* 733, *pp.* 504–527.
doi:10.1017/jfm.2013.452

Linear shape oscillations and polymeric time scales of viscoelastic drops

Günter Brenn† **and Stephan Teichtmeister**

Institute of Fluid Mechanics and Heat Transfer, Graz University of Technology, Inffeldgasse 25/F, 8010 Graz, Austria

(Received 8 July 2012; revised 14 August 2013; accepted 25 August 2013; first published online 25 September 2013)

We study small-amplitude axisymmetric shape oscillations of viscoelastic drops in a gas. The Jeffreys model is used as the rheological constitutive equation of the liquid, which represents a liquid with a frequency-dependent dynamic viscosity. The analysis of the time-dependent deformations caused by the oscillations yields the characteristic equation for the complex frequency, which describes the oscillation frequency and damping rate dependence on the viscous liquid behaviour and the stress relaxation and deformation retardation time scales λ_1 and λ_2 involved in the viscoelastic material law. The aim of this study is to quantify the influences of the two time scales on the oscillation behaviour of the drop and to propose an experimental method to determine one of the time scales by measuring damped oscillations of a drop. A proof-of-concept experiment is presented to show the potential and limitations of the method. Results show that values of λ_2/λ_1 from these measurements are orders of magnitude smaller than typical values used in simulations of viscoelastic flows.

Key words: capillary waves, drops, viscoelasticity

1. Introduction

The deformations of a drop surface due to shape oscillations may influence transport processes across the liquid–gas interface, such as the evaporation of the drop and the absorption of gases from the environment. Examples of technical processes where drop shape oscillations may be important are fuel injection and flue gas cleaning. For their relevance for transport processes, and for scientific interest, oscillations of liquid drops have been under investigation since the times of Rayleigh (1879), who derived the angular frequency $\alpha_{m,0} = \sqrt{m(m-1)(m+2)}\sqrt{\sigma/\rho a^3}$ of linear oscillations of mode m for an inviscid drop with density ρ, radius a and surface tension σ against an ambient vacuum. Rayleigh's work was extended by Lamb (1881), who included the influence of viscosity of the drop liquid and obtained the oscillation frequency and the rate of decay of the oscillations in the limits of very high and very low drop viscosity. Lamb (1932) also generalized Rayleigh's result by including the influence of a host medium with a non-negligible density ρ_o on the oscillations of an inviscid drop. He obtained a dependence of the angular frequency of oscillation on a weighted mean of the two densities, $\alpha_m \propto \sqrt{\sigma/[m\rho_o + (m+1)\rho]a^3}$. The proportionality factor depends on the

† Email address for correspondence: brenn@fluidmech.tu-graz.ac.at

mode number m. The most general case of an oscillating viscous drop immersed in another liquid with non-negligible density and viscosity was analysed by Miller & Scriven (1968). From their work, the characteristic equation for the oscillating drop emerges in the form of a determinant that must equal zero. For the various special cases of fluid behaviour, the equation reduces to the well-known results of previous works.

This brief survey of the existing literature on linear drop oscillations, which we restrict to the classical works, reveals work on drops of Newtonian liquids only. To date, the literature on the oscillations of non-Newtonian, e.g. viscoelastic, drops has been quite sparse. Bauer (1985) and Bauer & Eidel (1987) studied the oscillations of an immiscible viscoelastic spherical system. The authors found that, depending on the stress relaxation time of the liquid as compared to the period of the oscillation, the drop deformation may be more or less influenced by the liquid elasticity. Khismatullin & Nadim (2001) presented an extensive theoretical analysis of the characteristic equation for linear shape oscillations of viscoelastic drops in a vacuum, and found some interesting influences from the liquid material properties. For example, ranges of values of the relaxation Deborah number (De_1) and the Ohnesorge number (Oh) of the drop exist where the shape oscillations are due to the elasticity of the liquid, not due to surface tension.

In the present study, we sketch the theoretical derivation of the characteristic equation of the drop, quantifying the influence of viscoelasticity on the small-amplitude shape oscillations of drops of polymer solutions around their spherical equilibrium shape. We present an analysis of the importance of polymeric time scales for the motions, inspired by the results of Khismatullin & Nadim (2001). Ultimately we aim to propose the foundations of a method for measuring the deformation retardation time of the polymeric substance dissolved in the drop liquid using damped drop oscillations. To demonstrate its feasibility, we present and discuss a proof-of-concept experiment with first results that show that the deformation retardation time may depend on both the molecular properties and the concentration of the polymer in the solution.

Our paper is organized as follows. In the following section we sketch the theoretical derivation of the characteristic equation of the oscillating drop and the equations for the flow and pressure fields in the drop. In § 3 we analyse and discuss the characteristic equation of the oscillating drop in various states of motion caused by the relevant physical properties of the drop liquid. Section 4 presents the basics of an experimental method for measuring the polymer deformation retardation time and discusses various aspects of the experimental technique with influence on the results. In § 5 we summarize the article and draw the conclusions from the results.

2. Theoretical description of linear viscoelastic drop shape oscillations

Linear viscoelastic drop oscillations are described by the linearized equations of motion for an incompressible fluid and a linear viscoelastic material law. The appropriate material law is the Jeffreys model. The dependence of the motion on time is determined by an exponential function $\exp(-\alpha_m t)$, with the complex angular frequency α_m of mode m. The stress tensor $\boldsymbol{\tau}$ with this temporal behaviour satisfying the Jeffreys equation reads

$$\boldsymbol{\tau} = \eta_0 \frac{1 - \alpha_m \lambda_2}{1 - \alpha_m \lambda_1} \dot{\boldsymbol{\gamma}} = \eta(\alpha_m) \dot{\boldsymbol{\gamma}}, \tag{2.1}$$

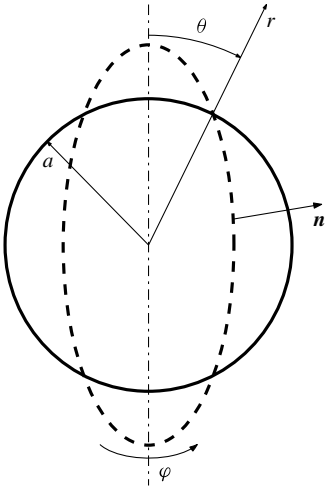

FIGURE 1. Equilibrium and deformed drop shapes in the spherical coordinate system for $m = 2$. The deformed shape given by the dashed line may be represented as $r_s(\theta, t) = a + \epsilon_0 P_m(\cos\theta)\mathrm{e}^{-\alpha_m t}$.

where λ_1 and λ_2 are the stress relaxation and deformation retardation times of the polymeric liquid, respectively, η_0 is the zero-shear viscosity and $\dot{\boldsymbol{\gamma}}$ is the rate-of-deformation tensor. With this material law, the structure of the momentum equation is formally identical to that for a Newtonian fluid, with the only difference being that the dynamic viscosity depends on the frequency of the deformations and on the two polymeric time scales λ_1 and λ_2.

We note that there exist several nonlinear rheological material models exhibiting the Jeffreys model as the linear limit. Among them we mention the Oldroyd eight-constant and the Giesekus models (Bird, Armstrong & Hassager 1987; Giesekus 1994). The latter includes the Oldroyd-B model as a special case and expresses the extra stress $\boldsymbol{\tau} = \boldsymbol{\tau}_s + \boldsymbol{\tau}_p$ and the dynamic viscosity $\eta = \eta_s + \eta_p$ as sums of contributions from the solvent and the polymer. The solvent stress $\boldsymbol{\tau}_s$ is formulated by the Newtonian material law, and the stress $\boldsymbol{\tau}_p$ due to the polymer is the solution of a differential equation with a convective derivative. The linear limit of the resulting differential equation for the total extra stress $\boldsymbol{\tau}$ is formally identical with the Jeffreys model and exhibits a factor corresponding to the deformation retardation time λ_2, leading to the equation $\lambda_2 := \lambda_{2G} = \lambda_1\eta_s/\eta_0$. It will be interesting to test the values λ_{2G} from this approach for their suitability for use with the characteristic equation of the oscillating drop in the present analysis.

The continuity and momentum equations are formulated in spherical coordinates and solved subject to the kinematic boundary condition that the rate of radial displacement of the drop surface $r_s(\theta, t)$ from the spherical equilibrium (figure 1) equals the radial velocity component at the location of the equilibrium drop radius a, and the dynamic boundary condition that the shear stress at the drop surface, evaluated at $r = a$, is zero in the present case of a drop in a gas. The normal-stress boundary condition will finally reveal the characteristic equation of the system.

The oscillation-induced flow in the drop is analysed assuming symmetry in the direction of the azimuthal angle φ. The description of the two-dimensional flow field is based on the Stokesian stream function ψ. Introducing it into the linearized

momentum equation by proper definition of the velocity components v_r and v_θ, and taking the curl of the resulting equation, the fourth-order partial differential equation

$$\left(-\frac{1}{\nu(\alpha_m)}\frac{\partial}{\partial t}+E^2\right)(E^2\psi)=0 \tag{2.2}$$

with the operator (Bird, Stewart & Lightfoot 1960)

$$E^2=\frac{\partial^2}{\partial r^2}+\frac{\sin\theta}{r^2}\frac{\partial}{\partial\theta}\left(\frac{1}{\sin\theta}\frac{\partial}{\partial\theta}\right) \tag{2.3}$$

is obtained. The solution of this equation reads

$$\psi=[C_{1,m}r^{m+1}+C_{2,m}qr\mathrm{j}_m(qr)]\sin^2\theta\, P'_m(\cos\theta)\mathrm{e}^{-\alpha_m t}, \tag{2.4}$$

where j_m is a spherical Bessel function of the first kind. In its argument we have defined

$$q=\sqrt{\alpha_m\rho/\eta(\alpha_m)}=\sqrt{\alpha_m/\nu(\alpha_m)}. \tag{2.5}$$

The resulting radial and angular components of the velocity vector read

$$v_r=-\left[C_{1,m}r^{m-1}+C_{2,m}q^2\frac{\mathrm{j}_m(qr)}{qr}\right]m(m+1)P_m(\cos\theta)\mathrm{e}^{-\alpha_m t} \tag{2.6}$$

and

$$v_\theta=\left[C_{1,m}(m+1)r^{m-1}+C_{2,m}q^2\left((m+1)\frac{\mathrm{j}_m(qr)}{qr}-\mathrm{j}_{m+1}\right)\right]\sin\theta\, P'_m(\cos\theta)\mathrm{e}^{-\alpha_m t}. \tag{2.7}$$

The two integration constants C_1 and C_2 are determined by the above-mentioned kinematic and dynamic boundary conditions. For the drop shape given in figure 1, the two conditions reveal the constants

$$C_{1,m}=\frac{\epsilon_0\alpha_m}{m(m+1)a^{m-1}}\left[1+\frac{2\left(m^2-1\right)}{2qa\mathrm{j}_{m+1}(qa)/\mathrm{j}_m(qa)-q^2a^2}\right] \tag{2.8}$$

$$C_{2,m}=-\frac{2(m-1)\epsilon_0\alpha_m a}{mq[2qa\mathrm{j}_{m+1}(qa)-q^2a^2\mathrm{j}_m(qa)]}. \tag{2.9}$$

This velocity field is formally identical with the results of Chandrasekhar (1959) and Khismatullin & Nadim (2001).

The pressure field is readily obtained with the known velocity field by integration of the momentum equation and reads

$$p=-(m+1)C_{1,m}\rho\alpha_m r^m P_m(\cos\theta)\mathrm{e}^{-\alpha_m t}. \tag{2.10}$$

The characteristic equation for the complex angular frequency α_m is found from the second dynamic boundary condition, which states that the (r, r) component of the total stress tensor vanishes at the drop surface. It reads

$$\frac{\alpha_{m,0}^2}{\alpha_m^2}=\frac{2(m^2-1)}{q^2a^2-2qa\mathrm{j}_{m+1}/\mathrm{j}_m}-1+\frac{2m(m-1)}{q^2a^2}\left[1+\frac{2(m+1)\mathrm{j}_{m+1}/\mathrm{j}_m}{2\mathrm{j}_{m+1}/\mathrm{j}_m-qa}\right]. \tag{2.11}$$

Here the spherical Bessel functions are taken at the value qa of their arguments. The equation is identical to the results of Lamb (1881) and Chandrasekhar (1959). In the present case of a viscoelastic liquid, however, the kinematic viscosity ν involved in

the equation is a function of the oscillation frequency α_m. In the following section we analyse the behaviour of the oscillating drop by solving this equation.

3. Analysis of the characteristic equation for a viscoelastic drop

To solve the characteristic equation (2.11), we introduce $\eta(\alpha_m)$ resulting from the linearized material law (2.1). For the analysis we use the definitions

$$y = \alpha_m/\alpha_{m,0}, \quad Oh = \eta_0/\sqrt{\sigma a \rho}, \quad De_1 = \alpha_{m,0}\lambda_1, \quad De_2 = \alpha_{m,0}\lambda_2, \tag{3.1}$$

which enter the argument qa of the spherical Bessel functions as per

$$q^2a^2 = \sqrt{m(m-1)(m+2)}\,\frac{y}{Oh}\,\frac{1-yDe_1}{1-yDe_2}. \tag{3.2}$$

Since α_m occurs in the argument of the spherical Bessel functions, it is not possible to solve the characteristic equation analytically. For a numerical analysis of (2.11) we use the computer algebra software MATHEMATICA.

Before starting the analysis, we validated our MATHEMATICA routine by reproducing some results of Khismatullin & Nadim (2001) for quadrupole oscillations $m = 2$. For a fluid characterized by $\rho = 10^3$ kg m^{-3}, $\sigma = 0.073$ N m^{-1}, $\eta_0 = 10^{-3}$ Pa s and a drop radius $a = 0.1$ mm, we obtain from Rayleigh's equation the angular frequency $\alpha_{2,0} \approx 24\,166$ s^{-1}. The Ohnesorge number defined in (3.1) equals 0.0117. The deformation retardation time λ_2 is set to zero, as Khismatullin & Nadim (2001) did in their investigation. Our results for the non-dimensional frequency and damping rate as functions of De_1 (not shown here) agree with figure 1 of Khismatullin & Nadim (2001). Without the liquid elasticity, one would expect the angular frequency to assume the value of $\alpha_{2,0}$ (Prosperetti 1980).

Taking the same Rayleigh frequency as before, and varying the Ohnesorge number as a parameter, we reproduce figure 4 of Khismatullin & Nadim (2001), which displays the dimensional frequency $f = [\mathrm{Im}(y)\,\alpha_{m,0}]/(2\pi)$ and the dimensional damping rate $d = \mathrm{Re}(y)\,\alpha_{m,0}$ as functions of the relaxation Deborah number De_1, again with $De_2 = 0$. Figure 2(*a*,*b*) displays these results. As the parameter in this analysis, Khismatullin & Nadim (2001) used a Reynolds number defined as $Re = a^2\alpha_{m,0}\rho/\eta_0$, which we rather interpret as an inverse of the Ohnesorge number Oh, since the angular frequency $\alpha_{m,0}$ depends on surface tension. The identity $Re = \sqrt{m(m-1)(m+2)}/Oh$ holds. For our case with $m = 2$, for example, $Oh = 11.8$ is equivalent to $Re = 0.24$. Khismatullin & Nadim (2001) pointed out that there exists a critical relaxation Deborah number De_1^* that marks the limit between the aperiodic mode of decay and the oscillatory mode. Figure 2(*a*) shows that this critical Deborah number increases with decreasing Ohnesorge number. We can also see this change in the damping behaviour in figure 2(*b*), which shows details of the drop behaviour beyond figure 4 of Khismatullin & Nadim (2001). While the damping rate increases with the Deborah number for the aperiodic cases, it decreases with further increase of the elasticity, once the critical Deborah number is exceeded. The rate of decay of deformations assumes lower values for high supercritical Deborah numbers than in the aperiodic cases.

We now present further results from an analysis of the characteristic equation (2.11). For this purpose, the deformation retardation time λ_2 of the fluid must be given a value. The deformation retardation time represents the time scale of relaxation of the rate of strain, once the stress is removed (Joseph 1990). To date, there is no established technique for measuring this time scale (Huang, Hu & Joseph 1998). What we know, however, is that the relation $\lambda_2 < \lambda_1$ must hold in order that the sign

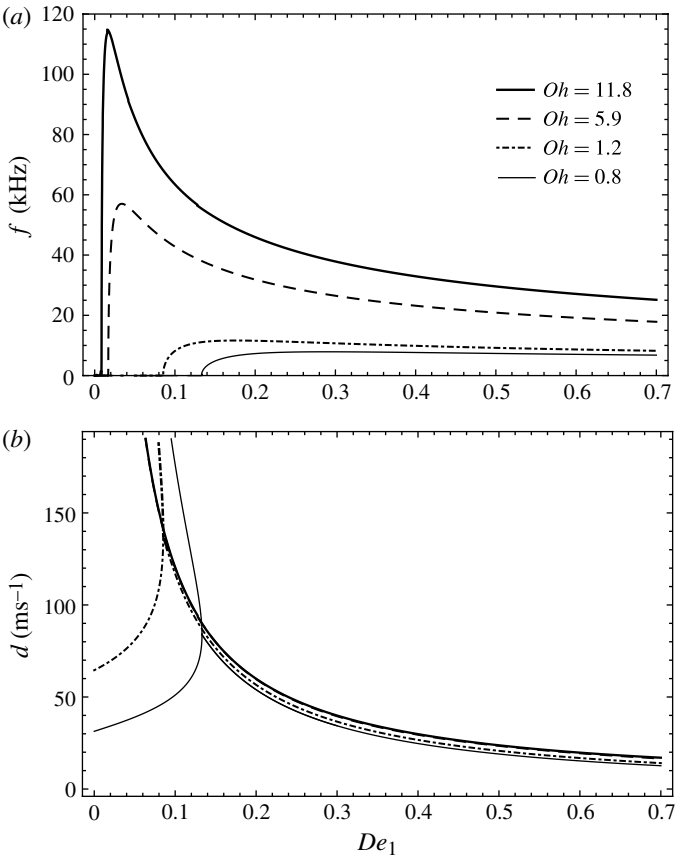

FIGURE 2. (*a*) Frequency and (*b*) damping rate as functions of the relaxation Deborah number for mode $m = 2$ with $\rho = 10^3$ kg m^{-3}, $\sigma = 0.073$ N m^{-1}, $\eta_0 = 1$ mPa s and drop radius $a = 0.1$ mm. The retardation time λ_2 was set to zero, as in Khismatullin & Nadim (2001).

of the extra stress is correct (Bird *et al.* 1987). The case where $\lambda_2 = \lambda_1$ represents a Newtonian fluid. For values of λ_2/λ_1 less than a threshold value, shear-thinning behaviour as predicted by the corotational Jeffreys model becomes excessive (Larson 1988). Larson gives the value of 1/8 for the threshold, whereas Denn (1990) and Giesekus (1994) give 1/9. In the literature, values for λ_2/λ_1 of 1/10 and 1/8 are commonly used, for historical rather than for physical reasons (Huang *et al.* 1998; Phillips & Williams 1999; Ho-Minh, Mai-Duy & Tran-Cong 2010). For the present part of our analysis we set $De_2 = De_1/10$. Our ultimate aim, however, is to propose a method for measuring λ_2 from damped drop oscillations (Trinh, Zwern & Wang 1982). We are therefore interested in the frequency and the damping rate as functions of the Ohnesorge number, with the relaxation Deborah number De_1 as a parameter (figure 3*a*,*b*). For the inelastic, Newtonian case ($De_1 = 0$), the non-dimensional frequency decreases with increasing Ohnesorge number. This means that, for example, an increase of the viscosity reduces the frequency. For Ohnesorge numbers exceeding the critical value $Oh_0^* \approx 0.766$, where the subscript 0 denotes the case of zero elasticity, two aperiodic modes of decay occur.

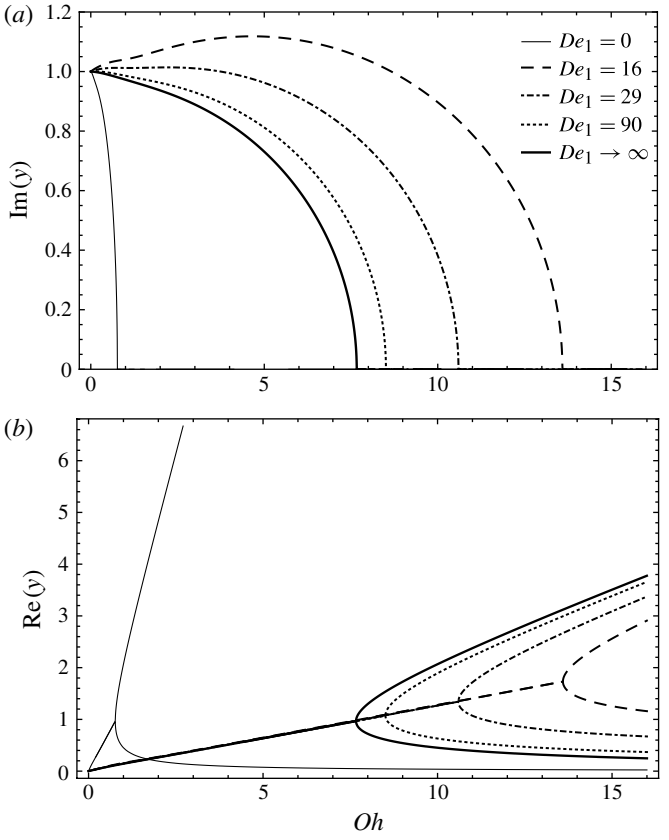

FIGURE 3. Non-dimensional (*a*) frequency and (*b*) damping rate as functions of the Ohnesorge number for mode $m = 2$.

Liquid elasticity ($De_1 > 0$) leads to greater values of Oh^* than the inelastic case and, therefore, to wider ranges of the Ohnesorge number where shape oscillations exist. It is important to note, however, that increasing elasticity makes this range narrower, for example, $Oh^*_{16} \approx 13.5$, while $Oh^*_{29} \approx 10.5$. The critical Oh number, however, does not reach the value of 0.766 of the purely viscous case, even for very large De_1. This convergence behaviour can be expected, since the curves approach the purely viscous one as the relaxation Deborah number increases, but the deformation retardation keeps the corresponding viscosity lower than in the inelastic case. Considering Oh^* as a function of De_1, we find that

$$\lim_{De_1 \to \infty} Oh^* \approx 7.66.$$

This is 10 times the value of the inelastic case, since, in the case that the ratio λ_2/λ_1 converges to a finite value not equal to zero as De_1 goes to infinity, $\lim_{De_1 \to \infty} \eta(\alpha_m) = \eta_0 De_2/De_1$, and we have set $\lambda_2 = \lambda_1/10$ for the present analysis. This behaviour is seen for each Ohnesorge number with shape oscillations: $\mathrm{Im}(y)$ decreases when the drop elasticity is increased, but there exists a lower limit of the non-dimensional frequency. For example, for $Oh = 6$, it is not possible to reach $\mathrm{Im}(y) < 0.6$ by increasing the elasticity. Finally, we may mention that the tendency of

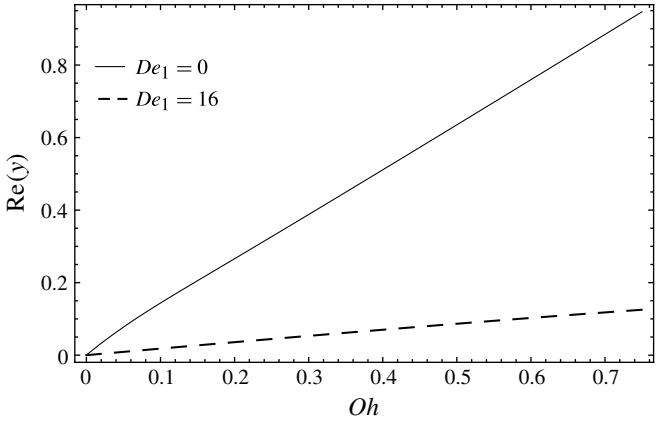

FIGURE 4. Non-dimensional damping rate in the range of subcritical Ohnesorge numbers for $m = 2$ at $De_1 = 0$ and 16. The slight bends mark the limits of validity of the low-viscosity approximation.

the frequency to decrease or increase depends on the degree of elasticity. For example, for the lowest Deborah number not equal to zero in figure 3(*a*), the frequency increases with Oh, reaches a maximum at $Oh \approx 5$, and then decreases again. This behaviour is not found for the higher De_1, where the frequency is monotonic with Oh.

Figure 3(*b*) shows the damping behaviour of the drop oscillations. For zero Ohnesorge number, i.e. for the inviscid case, the damping rate is zero, as expected. For $Oh < Oh^*$, the dependence on Oh appears to be linear. The dependence $\partial \mathrm{Re}(y)/\partial Oh$, however, assumes a smaller value in the interval $[0, Oh^*]$ of the Ohnesorge number than predicted by the low-viscosity limit (Khismatullin & Nadim 2001)

$$\left.\frac{\partial \mathrm{Re}(y)}{\partial Oh}\right|_{Oh\to 0} = \frac{(m-1)(2m+1)(1+De_1De_2)}{\sqrt{m(m-1)(m+2)}(1+De_1^2)}. \tag{3.3}$$

The straight line seen for $Oh < Oh^*$ bifurcates at Oh^* into two branches, with the lower one converging for $Oh \gg Oh^*$ to a line $\mathrm{Re}(y) \propto 1/Oh$. The bifurcation of the damping rate into a fast decaying (upper) and a creeping (lower) mode at the onset of aperiodic behaviour was found also by Chandrasekhar (1959) and by Prosperetti (1980) for the Newtonian case. Since the mode on the upper branch disappears very rapidly, it is not observed in experiments. It is, however, a part of the manifold of solutions of the characteristic equation of the drop in the aperiodic regime and therefore shown here. The inelastic curves in figure 3 are identical to the results by Prosperetti (1980). It is interesting to note that the apparently linear behaviour of the damping rate for subcritical Ohnesorge numbers is not really linear, as seen in figure 4, where we show the evolution of the damping rate with Oh for the inelastic case and for $De_1 = 16$. The bend in the curves is slight, but indicates the range of Oh numbers where the low-viscosity approximation is valid. For the inelastic case this range ends at $Oh \approx 0.06$, while it extends to 0.1 for $De_1 = 16$.

Considering the dependences for small Ohnesorge numbers $O(10^{-2})$, which may occur, for example, for drops with $a = 0.8$ mm, $\rho = 1000$ kg m^{-3}, $\sigma = 0.07$ N m^{-1} and η_0 between 2 and 10 mPa s, we obtain the data in figure 5(*a*,*b*). For very large stress relaxation times, we see the same trend as for the inelastic liquid. The non-dimensional angular frequency decreases with increasing Ohnesorge number of

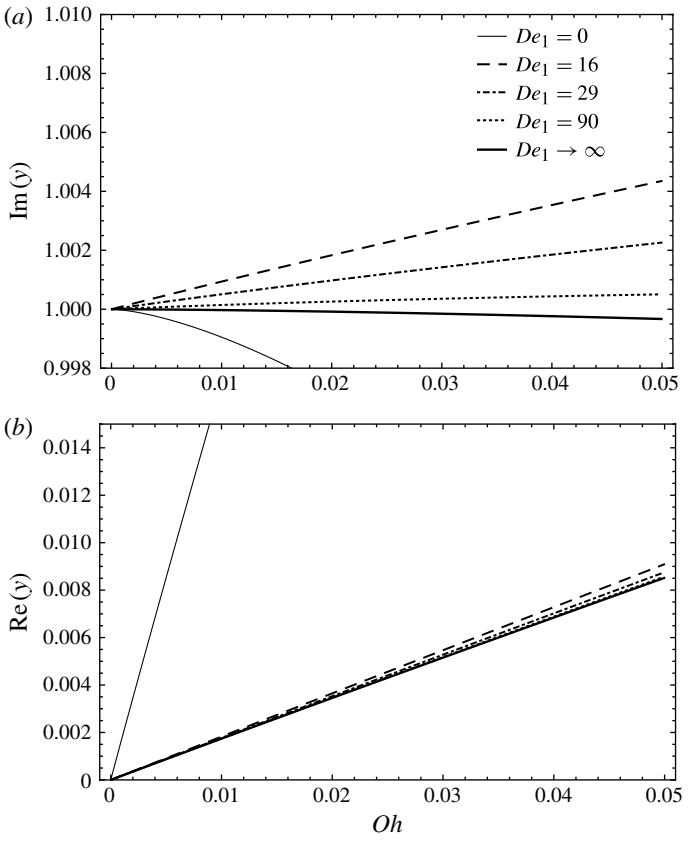

FIGURE 5. Non-dimensional (a) frequency and (b) damping rate for small Ohnesorge numbers for the mode $m = 2$.

the drop, i.e. with increasing liquid viscosity. This is, however, not the case for viscoelastic liquids with $De_1 < 90$. Here the elasticity causes frequencies above the Rayleigh frequency. In the low-viscosity limit, the damping rate is a linear function of Oh, as predicted by equation (43) of Khismatullin & Nadim (2001). For these small Oh, the line is steeper than in the range of Ohnesorge numbers up to Oh^*. From figure 4 we conclude for $De_1 = 16$ that the validity of the low-viscosity approximation is limited to $Oh \leqslant 0.1$. Since the curves $\mathrm{Re}(y) = f(Oh)$ nearly collapse for higher $De_1 > 16$ at small Oh, it is reasonable to assume that this limit applies to the higher relaxation Deborah numbers also.

We now analyse the behaviour of the characteristic equation (2.11) with varying Oh for small relaxation Deborah numbers. For the values of $De_1 \geqslant 16$ investigated so far, we have seen that, for decreasing De_1, the critical Ohnesorge number Oh^* increases, i.e. the range of subcritical Ohnesorge numbers enabling shape oscillations widens (figure 3a). For much smaller Deborah numbers De_1, however, the frequency may first decrease with increasing Oh, vanish, and, at a certain value of the Ohnesorge number, increase again with a sharp bend of the curve (figure 6). With decreasing Deborah number $De_1 < 1$, the state at the bend decreases to $\mathrm{Im}(y) = 0$, which it reaches at $De_1 \approx 0.2$ and $Oh \approx 0.6$. This state corresponds to the critical value of the stress relaxation time $\lambda_{1,c}$ given by Khismatullin & Nadim (2001). For values of

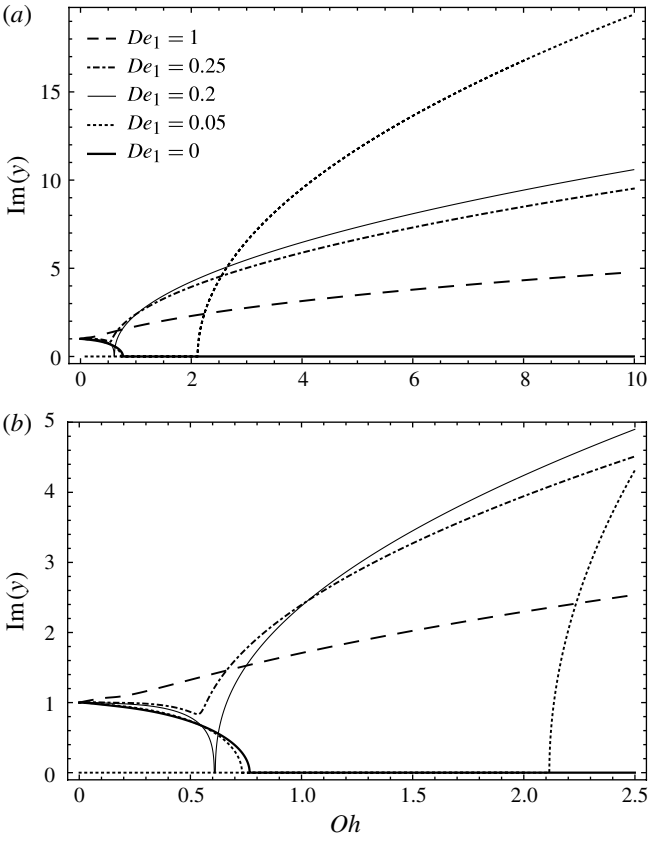

FIGURE 6. (*a*) The non-dimensional oscillation frequency for small Deborah numbers with $m = 2$. (*b*) Enlarged part of figure 6(*a*).

De_1 less than 0.2, a range of values of Oh with aperiodic drop behaviour is formed between two separate branches (figure 6*a*). The two branches represent states of the drop enabling shape oscillations. The branch at the higher Oh numbers represents oscillations that are due to the liquid elasticity, not due to the surface tension (Khismatullin & Nadim 2001). For these cases we can define a lower and an upper critical Oh number, which we term Oh_l^* and Oh_u^*, respectively. Figure 7 displays Oh_l^* and Oh_u^* as functions of De_1. The difference between the critical Oh numbers increases with decreasing Deborah number De_1. The maximum De_1 enabling this behaviour represents the critical stress relaxation time $\lambda_{1,c}$, which corresponds to the viscosity at the onset of elastic shape oscillations of the viscoelastic drop. In the present cases, where we have set $\lambda_2 = \lambda_1/10$, this phenomenon is observed for $0 < De_1 < 0.2$ only. Figure 8(*a*) shows the non-dimensional damping rate as a function of the Ohnesorge number for varying De_1, with a zoom-in displayed in figure 8(*b*). Here the critical states of the Ohnesorge number are also visible. In the range of small Oh, where shape oscillations exist, the damping rate varies approximately linearly with the Ohnesorge number, as for the much larger De_1 also. The dependence is nonlinear in the range of aperiodic drop behaviour (i.e. for Ohnesorge numbers between Oh_l^* and Oh_u^*). We discuss the case of $De_1 = 0.05$ given by the dotted curves in figure 8. The curves show three solutions of the characteristic equation, which correspond to the related dotted

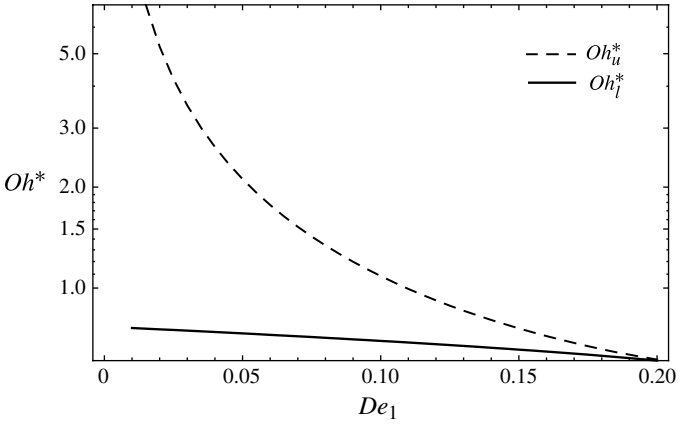

FIGURE 7. Lower and upper critical Ohnesorge numbers as functions of the relaxation Deborah number for $m = 2$.

curves for the oscillation frequency in figure 6. In figure 9 we put these solutions together: (i) the curve with shape oscillations, starting at $Oh = 0$ with the damping rate increasing up to the bifurcation point at $Oh \approx 0.6$ and then decreasing along the lower of the two aperiodic modes; (ii) the aperiodic upper branch from the bifurcation point at $Oh \approx 0.6$ up to the damping rate of $\sim$10 at $Oh \approx 2.1$, where a new branch appears with apparently linear increase of the damping rate with the Ohnesorge number (the latter corresponds to the branch of non-zero oscillation frequencies starting at $Oh \approx 2.1$); and (iii) the part of the upper aperiodic branch with damping rates $\geqslant$10 for Oh between $\approx$2.1 and 0 (the oscillation frequency corresponding to this branch in figure 6(*a*) is zero). This structure of the solution indicates that the shape oscillations at Oh numbers above $\approx$2.1 are damped more strongly than the aperiodic deformations on the upper branch of the bifurcation of an inelastic liquid.

Finally we look at the non-dimensional frequency and damping rate as functions of the Deborah number, with the Ohnesorge number as the parameter. We select values of the parameter that may be realized in experiments with acoustically levitated drops. The data are shown in figure 10(*a*,*b*). The non-dimensional frequency increases steeply with the Deborah number at small De_1, where the curves for all values of Oh investigated collapse. Higher Oh exhibit higher maximum non-dimensional frequencies. In the present range of Oh numbers, however, the maximum frequency deviates from the Rayleigh frequency by no more than 6 %. At high values of De_1, the non-dimensional frequency converges asymptotically to the value of 1, which is the state of the Rayleigh frequency. This means that, regardless of the value of the Ohnesorge number in the present range, the value of 1 is approached in all cases for high Deborah numbers De_1 above, say, 80. This behaviour corresponds to the finding that $\partial \mathrm{Im}(y)/\partial Oh$ is very small for small Oh at high relaxation Deborah numbers. The damping rate also converges to constant values with increasing Deborah number (figure 10*b*). The values assumed asymptotically are smaller for smaller Oh, as expected. The smaller Ohnesorge numbers lead to smaller damping rates, which is again reasonable. The drop behaviour is unaffected by stress relaxation times that are very long compared to the oscillation period. The liquid then behaves as Newtonian, with a viscosity influenced by the ratio λ_2/λ_1.

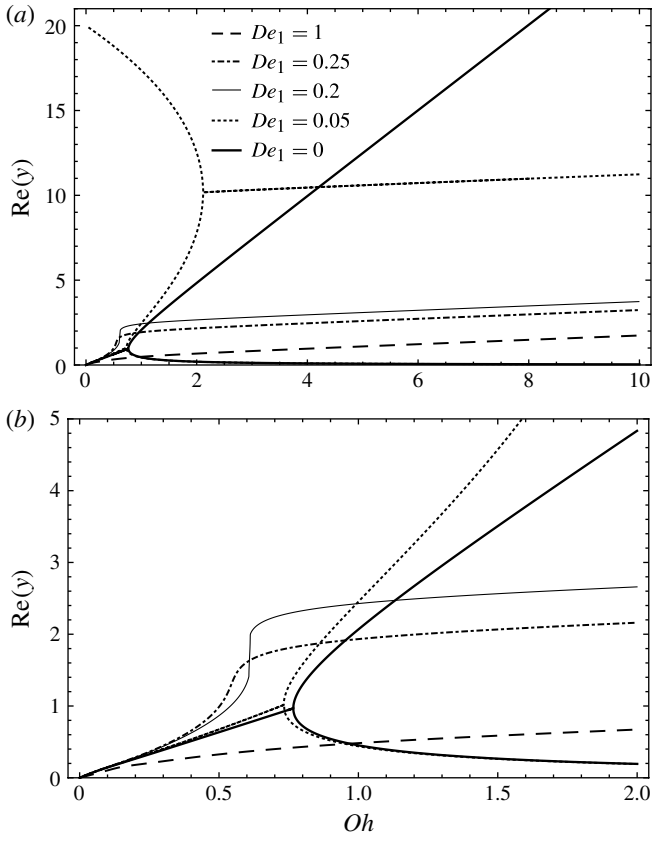

FIGURE 8. (*a*) The non-dimensional damping rate for small Deborah numbers at $m = 2$. (*b*) Enlarged part of figure 8(*a*).

4. An experimental approach to determine the deformation retardation time from damped drop oscillations

4.1. *Liquid characterization by the oscillating drop method*

The oscillating drop method has been developed and used in the past for measuring various physical liquid properties. The dynamic viscosity of aerodynamically levitated drops was measured by Perez *et al.* (2000) making use of the resonance behaviour of the oscillating drop with account for the spheroidal drop shape. The dynamic viscosity follows from a correlation with the width of the resonance peak, which the authors derive. The accurately measurable dynamic liquid viscosity ranges between 2 and 150 mPa s. The authors propose to apply the method to materials in the semisolid state (Perez *et al.* 2000). Similarly, Egry *et al.* (1998) used the damped oscillations of drops of the eutectic $Pd_{78}Cu_6Si_{16}$ for measuring the dynamic viscosity of the material over a wide temperature range. In this case, the drops were observed in microgravity, so that an extra levitation technique was not needed. At the eutectic temperature of 1033 K, the measured dynamic viscosity was found to agree very well with results known from the literature. Further to the dynamic viscosity of Newtonian systems, the oscillating drop method was applied to measure the surface tension of the drop liquid against the ambient air (Hiller & Kowalewski 1989) and the interfacial tension

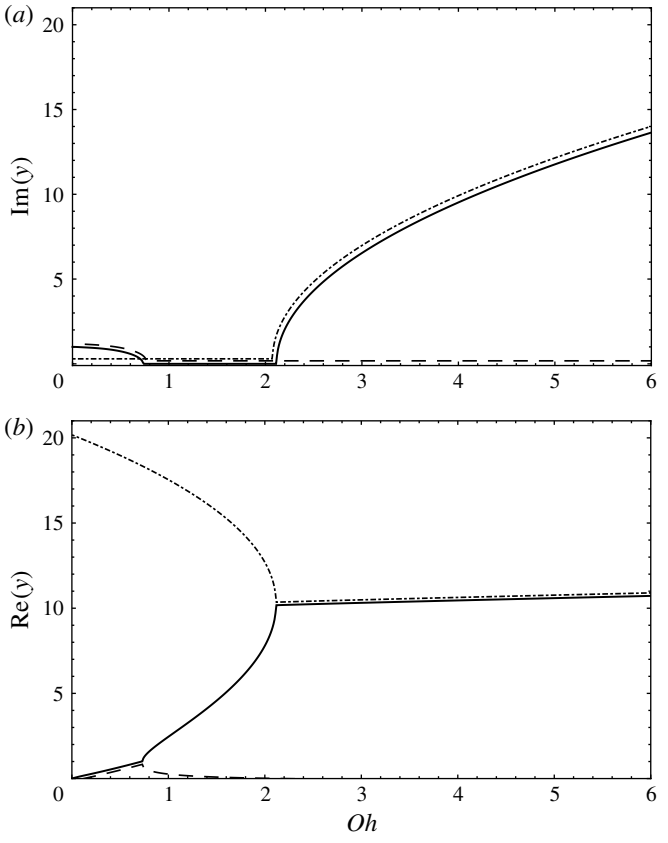

FIGURE 9. The non-dimensional (*a*) angular frequency and (*b*) damping rate at $De_1 = 0.05$ for $m = 2$: three solutions of the characteristic equation. The branches of the solution are slightly mutually displaced to make them more easily visible.

between immiscible liquids (Hsu & Apfel 1985). The former authors determined the drop oscillation frequency from drop images obtained by visualization; the latter determined the resonance frequency to derive the interfacial tension with the densities of the two liquids given.

For viscoelastic systems, the oscillating drop method was used for investigating the surface rheology (Tian, Holt & Apfel 1995; Apfel *et al.* 1997). The materials were surfactant solutions, and the drops were levitated due to the microgravity conditions of the experiment. In the study by Tian *et al.* (1995), complementary effects of the bulk and the surface viscosities were found. Owing to the coupling between the surface elastic and viscous effects, the surface viscosities can enhance or lower the damping rate of the drop. Experimental studies based on drop visualization under microgravity conditions determined the frequency and damping rate of free drop oscillations excited by loudspeakers. The experiments quantified both bulk and surface viscoelastic properties of surfactant solutions with the aim of developing rational models of the behaviour of the surfactants (Apfel *et al.* 1997). A study with crude oil in water used the oscillating pendant drop method to determine the dilatational elasticity modulus and the dynamic interfacial tension of the oil (Aske, Orr & Sjöblom 2002). The aim of that study was to quantify the absorption behaviour of crude oil

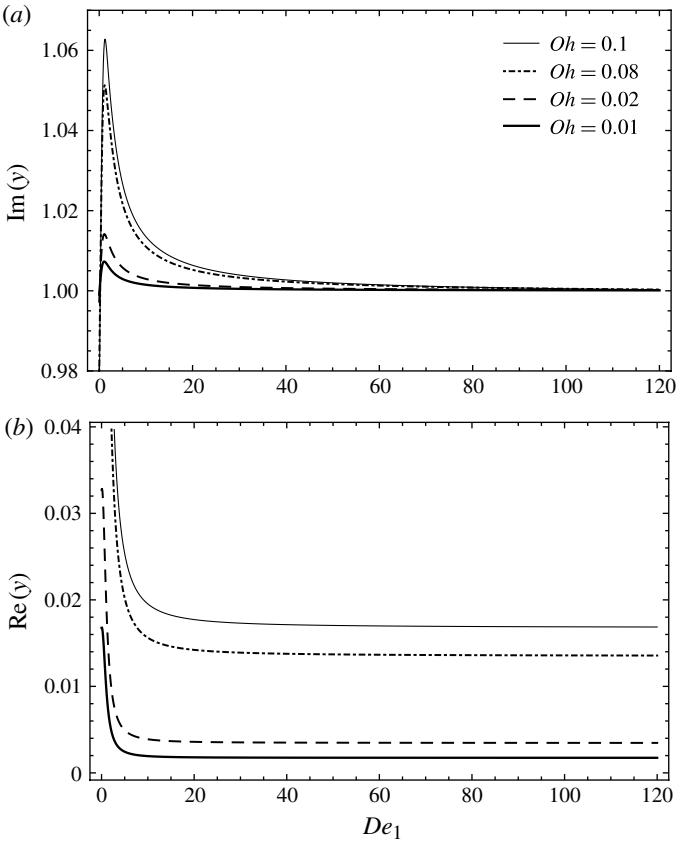

FIGURE 10. Non-dimensional (*a*) frequency and (*b*) damping rate as functions of the Deborah number De_1 ($m = 2$).

surfactants at oil–water interfaces. A review of oscillating drop and bubble techniques is given by Kovalchuk *et al.* (2001).

4.2. *Properties of the oscillating drop*

In the above analyses of the present study, the polymer deformation retardation time λ_2 was set to one-tenth of the stress relaxation time λ_1. While the latter may be determined experimentally with a standard method (Stelter *et al.* 2000) for spinnable polymer solutions, the former is far more difficult to obtain (Huang *et al.* 1998). The characteristic equation of the oscillating drop (2.11) involves both time scales, as well as a dynamic viscosity scale η_0, and we propose to use the characteristic equation for determining the values of η_0 and λ_2. This may be possible, since all the other quantities are given if both the frequency and the damping rate of oscillations of a drop of the polymeric liquid are known from an experiment. These quantities can be measured with acoustically levitated drops, as shown by Trinh *et al.* (1982) for a Newtonian drop embedded in an immiscible Newtonian host liquid.

Since our interest is to determine the deformation retardation time of a polymeric substance dissolved in a liquid, we look at solutions of the characteristic equation (2.11) for varying λ_2 and η_0 to quantify the sensitivity of the solutions against variations of these liquid properties. Varying the deformation retardation time in

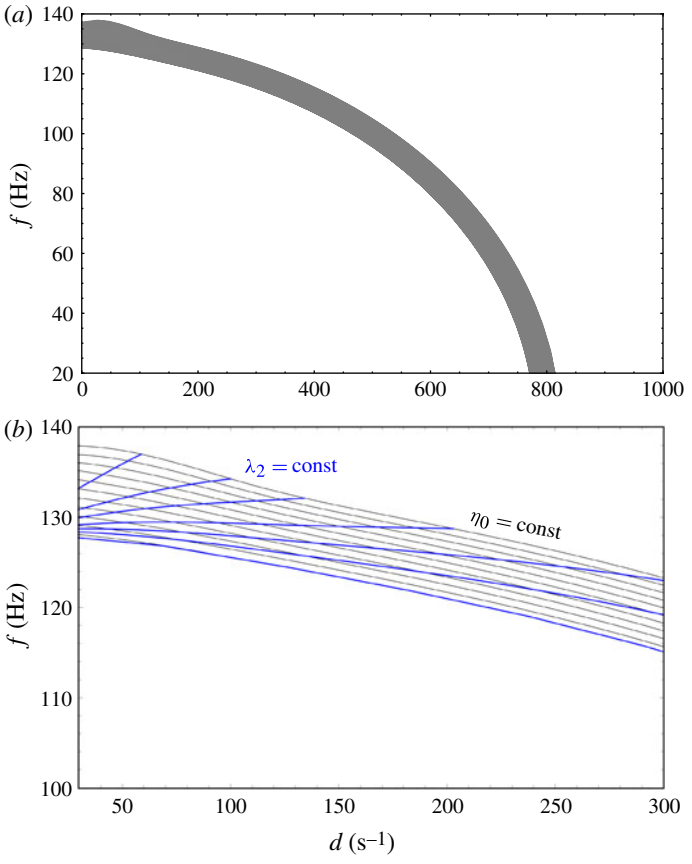

FIGURE 11. (Colour online) (*a*) Ranges of frequencies and damping rates for periodic oscillations of a 1.96 mm drop of an aqueous liquid with $\rho = 998.8\ \mathrm{kg\ m^{-3}}$, $\sigma = 0.0765\ \mathrm{N\ m^{-1}}$ and $\lambda_1 = 137.7$ ms ($m = 2$). (*b*) Enlarged part of figure 11(*a*) showing lines $\eta_0 =$ constant and $\lambda_2 =$ constant.

the range $3.3 \times 10^{-4}\,\lambda_1 \leqslant \lambda_2 \leqslant \lambda_1$ and the viscosity in the range 2×10^{-2} Pa s $\leqslant \eta_0 \leqslant 1.52$ Pa s for a drop with $\rho = 998.8\ \mathrm{kg\ m^{-3}}$, $\sigma = 0.0765\ \mathrm{N\ m^{-1}}$, $\lambda_1 = 137.7$ ms, $a = 0.98$ mm and $m = 2$, we obtain the results in figure 11(*a*). We see that the dimensional frequencies and damping rates cover a band in the Gaussian plane of the real and imaginary parts, d and f, of the complex angular frequency. A zoom-in to the range of damping rates $O(10^2\ \mathrm{s^{-1}})$ at frequencies $110\ \mathrm{Hz} \leqslant f \leqslant 140$ Hz is shown in figure 11(*b*). We see lines of constant viscosity η_0 and constant deformation retardation time λ_2. The dynamic viscosity varies from 0.02 Pa s on the bottom line, which ends at $d = 88\ \mathrm{s^{-1}}$, and in steps of 0.15–1.52 Pa s on the top line. The deformation retardation time on the lines from top to bottom assumes the values 4.59, 9.18, 13.77, 22.95, 36.72, 68.85 and 137.7 ms. The state $\lambda_2 = \lambda_1$ on the bottom line is not realized physically. These data represent that, with the values of oscillation frequency and damping rate known, the state of the drop defined by the pair of values (η_0, λ_2) may be determined by finding the point in this Gaussian plane.

The variation of the functions $\eta_0 = g_\eta(f, d)$ (say) and $\lambda_2 = g_\lambda(f, d)$ with their independent variables determines the accuracy of the measurements of f and d

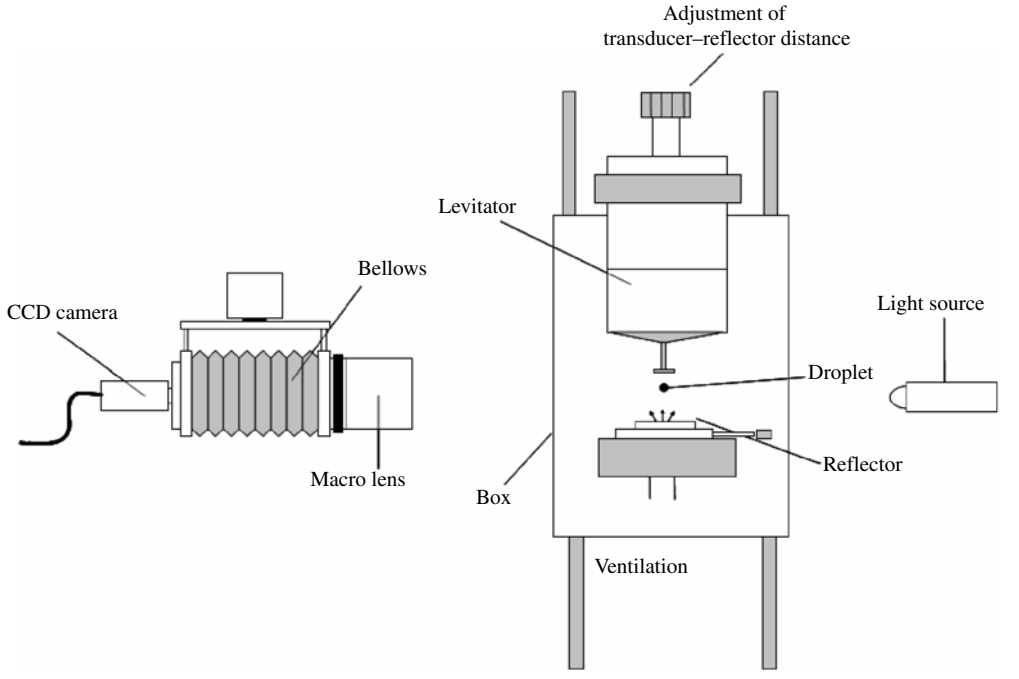

FIGURE 12. Set-up for levitating single drops in an ultrasonic resonator and measuring the drop deformations in forced oscillations by means of image processing.

required for a valid determination of η_0 and λ_2. Based on figure 11(*b*), we evaluate the dependences of η_0 and λ_2 with varying f and d. As an example, in the range around $f = 132$ Hz and $d = 30\ \mathrm{s}^{-1}$ we obtain that an uncertainty of $\pm 1\,\%$ in both the frequency and the damping rate results in uncertainties in η_0 and λ_2 of ± 30 and $\pm 40\,\%$, respectively. This means that the frequency and damping rate of the drop oscillations must be accurately measured in the experiment with uncertainties well below $1\,\%$.

4.3. *Acoustic drop levitation as the key experimental technique*

To investigate the damped oscillation behaviour of single drops of viscoelastic liquids experimentally, one may use the technique of acoustic levitation (Yarin *et al.* 1999). This technique allows for the positioning of individual drops in the quasi-steady pressure field of a standing ultrasonic wave produced between a vibrating horn and a reflector, as shown in figure 12. The reflector may have a concave curved surface to enhance the sound pressure level (SPL), as in the present apparatus. Oscillations of the levitated object may be excited by amplitude modulating the ultrasound. Modulation frequencies up to 2 kHz are achievable with the equipment at hand. For further details the reader is referred to Yarin *et al.* (1999).

A proof-of-concept experiment was carried out with aqueous solutions of the two different polyacrylamides, Praestol 2500 and Praestol 2540, from Stockhausen Inc. (Germany). The former is non-ionic with a degree of hydrolysis of 3–4 %, while the latter is middle anionic with a degree of hydrolysis of 40 %. The different degrees of hydrolysis of the polymers cause different mechanical flexibilities of the macromolecules. The molecular weights are about the same for the two polymers,

Polymer	Solute mass fraction (wt %)	Density, ρ (kg m^{-3})	Surface tension, σ (N m^{-1})	Zero-shear viscosity, η_0 (Pa s)	Stress relaxation time, λ_1 (s)
Praestol 2500	0.3	999.4	0.07315	0.0435	0.078
	0.8	1000.9	0.07555	0.7588	0.163
Praestol 2540	0.05	998.8	0.07651	1.521	0.1377

TABLE 1. Properties of the three aqueous polymer solutions at 20 °C. The viscosity η_0 was measured with a rotational viscosimeter.

(15–20) $\times$ 10^6 kg kmol^{-1}. The properties of three aqueous solutions of these polymers relevant for the present study are listed in table 1.

Levitated drops of the solutions are produced by a syringe with a thin needle to enable the formation of drops with diameters in the range between 1.5 and 2.5 mm. With the needle tip close to a pressure node of the acoustic levitator, a portion of liquid is pushed out from the syringe to form the droplet. The drop resonance frequency is then determined approximately by a modulation frequency sweep, monitoring the maximum occurring oscillatory drop deformations. The drop is then steadily driven at that resonance frequency, and the modulation is switched off at a time $t = 0$, so that the drop carries out damped oscillations, which eventually die out.

4.4. *Visualization of the drop*

The damped oscillatory motion of the levitated drop is recorded by a high-speed camera at a frame rate of 2 kHz under backlight illumination. An uncertainty in the length measurement of ± 2 pixels with resolution of 167 pixels mm^{-1} results in a sizing uncertainty of ± 12 μm, for a 1.9 mm drop equivalent to ± 0.6 %. Within at most 10 s after the drop has been placed in the acoustic levitator, one single picture of the drop is taken in order to have its initial shape and volume. This initial state, where evaporation of the solvent has not yet had any influence on the solution concentration, allows the concentration of the drop liquid at all later times to be deduced from the volume. The proof-of-concept experiment showed that the maximum decrease of the drop volume observed between the initial state and later states after the frequency sweep is of the order of -15 %, which causes the same increase of the polymer concentration. The related increase of the zero-shear viscosity of the liquid depends on the polymer. For the two polyacrylamides studied in the present experiment, we see that η_0 may increase by 25–40 % due to solvent evaporation. The zero-shear viscosity obtained from the experiment is the value corresponding to the concentration of the solution present during the related experiment.

The oscillation shown in figure 13 was recorded for a Praestol 2500 solution drop with an equilibrium diameter of 1.94 mm. The drop was driven at 120 Hz before the modulation was switched off. From these data, the frequency and damping rate in the last part of the motion were extracted, so that both the linear oscillation behaviour was ensured and the shear thinning of the polymer solution did not have any influence on the oscillation. The real and imaginary parts of the complex angular frequency of this drop are therefore known.

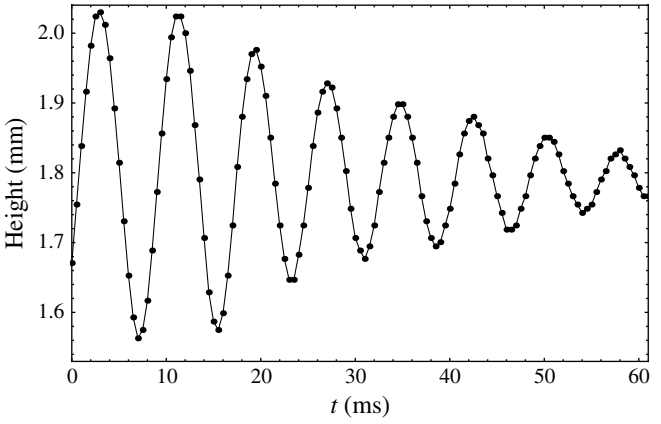

FIGURE 13. Distance between north and south poles of a levitated 1.94 mm 0.3 wt % Praestol 2500 solution drop as a function of time in a damped oscillation. Resolution is 167 pixels mm^{-1}. The time between two images is 0.5 ms.

4.5. *Uncertainty estimates*

The experiment presently proposed for determining the polymeric deformation retardation time from damped drop oscillations is subject to influences from the experimental method of acoustic levitation and the non-Newtonian behaviour of the polymeric liquid, which is shear thinning in many cases. In order to fulfil the limitations set by the linear theory underlying the characteristic equation of the drop, and in order to avoid influences from the shear thinning of the liquid, we measure the drop oscillation frequency and damping rate in the late stages of the damped oscillation. The proposed method, however, is still subject to some particularities that must be accounted for in the interpretation of the data. In the present section we discuss these aspects and their potential influence on the measurements.

4.5.1. *Acoustic streaming in the drop*

The steady flow induced by the unsteady boundary layer flow of the air around the drop in the acoustic levitator, called *acoustic streaming*, induces a recirculating liquid motion inside the drop due to shear forces on the drop surface. The velocity field in the drop induced by the acoustic streaming was calculated by Yarin *et al.* (1999). The maximum angular liquid velocity induced at the drop surface is given by the equation (Yarin *et al.* 1999)

$$v_{\theta,as}\big|_{r=a} = \frac{9}{80\sqrt{2}}\left(\frac{a}{\eta_0}\sqrt{\rho_a\eta_a\omega_{lev}}\right)\frac{B^2}{\omega_{lev}a}, \tag{4.1}$$

where ρ_a and η_a are the density and dynamic viscosity of the air, respectively, ω_{lev} is the angular frequency of the sound in the acoustic levitator, corresponding to the vibration frequency of the transducer of 58 kHz, and $B \approx 10^{-2}\omega_{lev}a$ is the amplitude of the gas particle velocity. For the example of a drop of the 0.3 wt % aqueous solution of Praestol 2500 in table 1, the velocity given by (4.1) is $O(0.2\ \mathrm{mm\ s}^{-1})$. As a comparison, the liquid velocity v_θ that results from (2.7) due to the oscillation in a late stage of the damped motion relevant for the measurement, where the non-dimensional deformation amplitude is $\approx 0.04a$, amounts to $O(12\ \mathrm{mm\ s}^{-1})$, which is two orders of magnitude higher. Since $v_{\theta,as}|_{r=a}$ is proportional to η_0^{-1}, the acoustically induced

velocity in the drop would remain negligible against the oscillation-induced velocity even for a one order of magnitude smaller liquid zero-shear viscosity. It should be noted that the above estimate was carried out for the lowest liquid dynamic viscosity investigated.

4.5.2. *Influence of the oblate drop shape on the oscillation frequency*

The theoretical analysis on which we base our study assumes a spherical equilibrium state of the oscillating drop. In acoustic levitation of drops, however, the sound pressure compensating the weight of the drop may cause its equilibrium shape to be more or less different from spherical. The deviation from the spherical shape depends on the SPL in the levitator and on the Eötvös number $Eo = g(\rho - \rho_0)a^2/\sigma$ of the drop. Small values of Eo allow for nearly spherical levitated drops. In the present proof-of-concept experiment, the static (aspect) ratios of the short to the long axes of the elliptical meriodional section of the oblate drop shape are $O(0.9)$, i.e. close to unity. For drops with a static oblate deformation, Trinh *et al.* (1982) investigated the shift of the resonance frequency from the value for the spherical drop and found an increase with decreasing aspect ratio. For the present values, Trinh *et al.* (1982) found a shift of the resonance frequency of $O(8\,\%)$. In their experiments, however, which were carried out with drops in immiscible liquid–liquid systems, the viscous and inertial influences from the ambient host medium on the drop oscillation are much stronger than in the present case of oscillations in a gaseous environment. We therefore expect a substantially lower influence of a non-spherical equilibrium drop shape on the resonance frequency here.

4.5.3. *Influence of the oscillation amplitude on the oscillation frequency*

It is well known that the nonlinear behaviour of oscillating drops at sufficiently large oscillation amplitudes changes the oscillation frequency and the times spent in the oblate and prolate states for the quadrupole mode of oscillation. Tsamopoulos & Brown (1983) found for inviscid drops that, for drop aspect ratios $O(1.5)$ in the maximum prolate state, the oscillation frequency decreases by 5 % from the Rayleigh value, and the time spent in the prolate shape increases to 57 %. In the present proof-of-concept experiment, the distortion of the drop in the period of time where the oscillation is measured is substantially lower than that, so that this nonlinear aspect will not be of any importance for the interpretation of the data.

4.5.4. *Influence of shear thinning of the liquid*

The linear analysis of the drop oscillations does not account for the rheological shear-thinning behaviour of the drop liquid. The dynamic viscosity η_0 in the Jeffreys model may be interpreted as the liquid zero-shear viscosity. The oscillatory liquid motion in the drop must therefore fulfil the requirement that shear rates be sufficiently small so as to avoid any influence from the shear thinning on the oscillations. This requirement coincides with the need for linearity of the drop oscillation behaviour. The shear stress relevant for the axisymmetric oscillations is $\tau_{r\theta}$. The relevant shear rate reads

$$\begin{aligned}\dot{\gamma}_{r\theta,m} &= \frac{1}{r}\frac{\partial v_r}{\partial \theta} + r\frac{\partial (v_\theta/r)}{\partial r} \\ &= \left[2(m^2-1)C_{1,m}r^{m-2} + 2C_{2,m}q^3\left(\frac{\mathrm{j}_m(qr)}{q^2r^2}(m^2-1) + \frac{\mathrm{j}_{m+1}(qr)}{qr} - \frac{\mathrm{j}_m(qr)}{2}\right)\right] \\ &\quad \times P'_m(\cos\theta)\sin\theta\,\mathrm{e}^{-\alpha_m t},\end{aligned} \tag{4.2}$$

where the real part is physically relevant. For the value $m = 2$ this relation becomes

$$\dot{\gamma}_{r\theta,2} = \left[6C_{1,2} + 2C_{2,2}q^3\left(3\,\frac{\mathrm{j}_2(qr)}{q^2r^2} + \frac{\mathrm{j}_3(qr)}{qr} - \frac{\mathrm{j}_2(qr)}{2}\right)\right] 3\cos\theta\sin\theta\,\mathrm{e}^{-\alpha_2 t}. \quad (4.3)$$

The integration constants $C_{1,m}$ and $C_{2,m}$ in this equation depend linearly on the deformation amplitude ϵ_0. With the complex angular frequency given as $\alpha_2 = \alpha_r + \mathrm{i}\alpha_i$, we require $\epsilon_0 \exp(-\alpha_r t)$ to be small enough to ensure a small shear rate. As the criterion for comparison of values of the shear rate with material data, we take the value at the onset of shear thinning. The latter is $O(1\ \mathrm{s}^{-1})$ for the 0.3 % Praestol 2500 solution, and one order of magnitude smaller for the 0.8 % Praestol 2500 and 0.05 % Praestol 2540 solutions. Our method is therefore applicable preferentially with dilute or semi-dilute polymer solutions that exhibit a high onset shear rate for the shear thinning.

As a quantity relevant for the integral behaviour of the drop, one may consider the time and volume average shear rate in the drop. Computing the shear rate in the drop as a function of the radial coordinate, we see that it changes its sign at up to nine locations in the drop. For the effect of the shear thinning of the liquid on the motion of the drop, the sign of the shear rate is unimportant. We therefore compute the time and volume average shear rate in the drop taking the absolute value of the integrand. As the averaging period we take the time interval in the measurement data used for determining the complex frequency α_2. Denoting the radially dependent part on the right in (4.3) as $K_r + \mathrm{i}K_i$, and the complex angular frequency as $\alpha_2 = \alpha_r + \mathrm{i}\alpha_i$, we obtain

$$\mathrm{Re}(\langle\bar{\dot{\gamma}}_{r\theta,2}\rangle) = \frac{3}{a^3}\frac{\Delta r_{inst}}{n}\int_{t^*=0}^{n}\int_{r=0}^{a}|K_r\cos 2\pi t^* + K_i\sin 2\pi t^*|\,r^2\mathrm{e}^{-2\pi t^*\alpha_r/\alpha_i}\,\mathrm{d}r\,\mathrm{d}t^*. \quad (4.4)$$

Here we have defined the non-dimensional time $t^* = t/T_2$. The displacement Δr_{inst} is the instantaneous deformation of the drop at the beginning of the time interval of the frequency measurement. To evaluate the real part of this equation, we make use of the time-dependent drop shape data recorded by the high-speed camera. For late times during the damped motion we get typical displacements of the drop north pole against the equilibrium shape Δr_{inst} of $O(30\ \mu\mathrm{m})$, corresponding to 5 pixels. The resulting shear rates averaged in space and time are $O(15\ \mathrm{s}^{-1})$. For the polymer solutions investigated here, this shear rate is greater than the values at the onset of shear thinning. These average values therefore do not reflect the experimental finding that the measurements may nonetheless yield correct results. In contrast, looking at the local shear rates in the drop, we see that, at every instant in time, drops yielding correct results exhibit the maximum shear rates in a region r/a around 0.8, while drops yielding viscosities η_0 deviating strongly from the viscosity measured with a shear rheometer exhibit the maximum of the shear rate in the centre of the drop. The shear rate at the droplet centre $r = 0$ is the real part of

$$\dot{\gamma}_{r\theta,2}\big|_{r=0} = (C_{1,2} + \tfrac{1}{15}C_{2,2}q^3)\,9\sin 2\theta\,\mathrm{e}^{-\alpha_2 t}. \quad (4.5)$$

Shear rate profiles at one time for $\theta = \pi/4$ are shown in figure 14 for drops of the three liquids in table 1. Typical values of the extreme shear rates are $O(20\text{–}60\ \mathrm{s}^{-1})$ at the drop centre, and $O(20\ \mathrm{s}^{-1})$ at the periphery. Resulting shear rates causing shear-thinning effects on the drop are not detrimental to the measurement if they occur at the drop periphery, while they are influential when located at the drop centre. The reason for this difference is that the part of the drop volume with its motion influenced

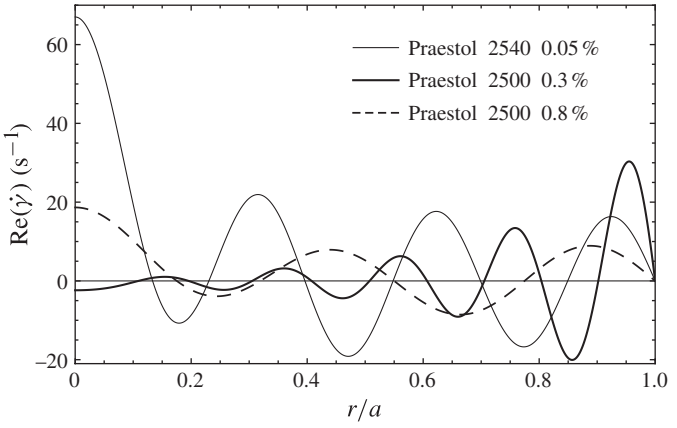

FIGURE 14. Profiles of the real part of the shear rate $\dot{\gamma}_{r\theta,2}$, here termed $\mathrm{Re}(\dot{\gamma})$, in drops of the three liquids in table 1. The drop sizes are 1.96, 1.94 and 1.85 mm for the three liquids from top to bottom; the corresponding drop Ohnesorge numbers are 5.6, 1.6 and 2.9.

by the shear thinning is large when high shear rates occur at the drop centre, and small when they occur at the periphery of the drop. We see in this finding an effect from the non-viscometric kinematics of the flow field in the drop. From these findings we may conclude that there exists a maximum allowable concentration for a given polymer, leading to a largest drop Ohnesorge number with tolerable dynamic influence on the drop shape oscillations in the sense of the present measurements.

4.6. *Evaluation of the characteristic equation and results from the proof-of-concept experiment*

In our proof-of-concept experiment, typical drop sizes were 2 mm. The drop Ohnesorge numbers range between 1.6 and 5.7. The polymer concentrations investigated yield zero-shear viscosities $O(0.04\ \mathrm{Pa\ s})$ and $O(0.76\ \mathrm{Pa\ s})$ for the two flexible polymer solutions, and $O(1.5\ \mathrm{Pa\ s})$ for the rigid, rod-like polymer solution (table 1). Stress relaxation times λ_1 were $O(0.1\ \mathrm{s})$. In the evaluation of the drop oscillations, we find oscillation frequencies $O(130\ \mathrm{Hz})$ and damping rates $O(1\ \mathrm{s}^{-1})$. In experimental cases where the resulting argument qa of the Bessel functions in the characteristic equation of the drop is large enough so that the relation $2(m+2)\mathrm{j}_{m+1}(qa)/\mathrm{j}_m(qa) \ll qa$ holds for both the real and the imaginary parts of the two complex relation partners, the approximation of the characteristic equation by its 'low-viscosity limit' (Khismatullin & Nadim 2001)

$$[\alpha_m^2 + \alpha_{m,0}^2]q^2a^2 = 2(m-1)(2m+1)\alpha_m^2 \tag{4.6}$$

may be used to determine η_0 and λ_2. This equation is cubic in the complex angular frequency α_m, but linear in η_0 and λ_2. With the complex frequency $\alpha_2 = \alpha_r + \mathrm{i}\alpha_i = d + \mathrm{i}2\pi f$ of the drop known, the two liquid properties are readily determined from the real and imaginary parts of (4.6), which yield

$$\eta_0 = \left[\frac{\lambda_1}{\alpha_{m,0}}(\alpha_r^2+\alpha_i^2) - \lambda_1\alpha_{m,0} + \frac{2\alpha_{m,0}\alpha_r}{\alpha_r^2+\alpha_i^2}\right]\frac{\sqrt{m(m-1)(m+2)}}{2(m-1)(2m+1)}\sqrt{\sigma a\rho} \tag{4.7}$$

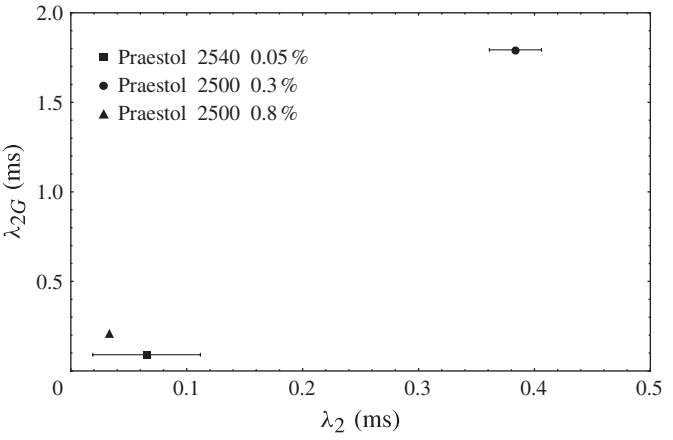

FIGURE 15. Pairs of time scales λ_2 from (2.11) and λ_{2G} as derived from the Giesekus model for the three polymer solutions in table 1.

and

$$\lambda_2 = \frac{1}{2\alpha_r} + \frac{\lambda_1(3\alpha_r - \alpha_i^2/\alpha_r)/2 + \alpha_{m,0}^2\lambda_1/2\alpha_r - 1}{\lambda_1(\alpha_r^2 + \alpha_i^2) - \lambda_1\alpha_{m,0}^2 + 2\alpha_{m,0}^2\alpha_r/(\alpha_r^2 + \alpha_i^2)}. \tag{4.8}$$

In the present proof-of-concept experiment, we see that the requirement for applicability of the low-viscosity limit (4.6) for determining the two liquid properties is satisfied very well by the real parts of the relation partners, but not by the imaginary parts. In consequence, we get very good agreement with deviations from the solution of the full equation (2.11) of $O(3\,\%)$ for the viscosity η_0, while the retardation times λ_2 determined by (4.8) exhibit deviations of $O(9\text{–}80\,\%)$. Here we therefore present the results from the evaluation of the full characteristic equation, although in the present state of development of the method the identification of the right solution among the values provided by the MATHEMATICA solver requires some manual intervention.

From the experiment with the 0.3 % Praestol 2500 solution drop of figure 13, we obtain the oscillation frequency $f = 128.4$ Hz $\pm$ 0.34 % and the damping rate $d = 1.308\ \mathrm{s}^{-1} \pm 2.9\,\%$. Using these data for solving the characteristic equation numerically, we obtain the pair $(\eta_0, \lambda_2) = (0.043\ \mathrm{Pa\ s} \pm 1.64\,\%,\ 0.384 \times 10^{-3}\ \mathrm{s} \pm 5.9\,\%)$. Equations (4.7) and (4.8) yield $(\eta_0, \lambda_2) = (0.04265\ \mathrm{Pa\ s} \pm 0.54\,\%,\ 0.4285 \times 10^{-3}\ \mathrm{s} \pm 3\,\%)$. The viscosity η_0 agrees very well with the value in table 1 measured as the first Newtonian plateau viscosity with a shear rheometer at shear rates below $1\ \mathrm{s}^{-1}$. The deformation retardation time obtained is two orders of magnitude below the stress relaxation time, which is reasonable for flexible macromolecules such as the present ones.

A set of deformation retardation times of the three aqueous polymer solutions in table 1 is shown in figure 15, where values obtained as solutions of the characteristic equation (2.11) are compared with values of the deformation retardation time $\lambda_{2G} = \lambda_1\eta_s/\eta_0$ from the Giesekus model. In the calculation of λ_{2G}, the value of the solvent viscosity used was 1 mPa s, and for η_0 the values from table 1 were taken. Although these data should be regarded as a first set of results, the values show clearly that the usual practice in simulations of viscoelastic flows to assume values of the ratio λ_2/λ_1 between 1/10 and 1/8 may miss the correct value substantially. Furthermore, a comparison of the measured values of λ_2 with the values

predicted by the linear limit of the Giesekus model yields strong deviations, the ratios λ_{2G}/λ_2 ranging between 0.5 and 6. The deviations are smaller for the hydrolysed rigid polymer than for the non-ionic flexible one, and increase with the polymer concentration in the solution. In turn, solving the characteristic equation (2.11) of the drop using the deformation retardation time λ_{2G} yields an oscillation frequency deviating from the measured value by less than 5 %, while the damping rate is missed by more than 280 %, which cannot be explained by inaccuracies of our measured data. This finding indicates clearly the need for the measured data of λ_2 and their value in characterizing the molecular influences on the deformation retardation behaviour of the solution. Since the mechanical flexibility of the macromolecules, which is influenced by the distribution of electrical charge on the molecules and the length of Kuhn segments, may differ strongly between ionic and non-ionic polymers and depend on the degree of hydrolysation of the molecules, a method for determining experimentally the deformation retardation time of the polymers in the solution is definitely needed. Work is under way to establish this method for determining deformation retardation times of polymers in solutions by an evaluation of damped drop oscillations.

5. Conclusions

In this study we analyse linear oscillations of viscoelastic drops. The damping rate as well as the oscillation frequency are found as solutions of the characteristic equation of the drop depending on the viscous and capillary liquid behaviour and the stress relaxation and deformation retardation time scales involved in the linearized constitutive rheological equation. An analysis of the characteristic equation shows that linear viscoelastic drop oscillations exhibit behaviours caused by the viscoelastic time scales, which lead to substantial differences from the Newtonian behaviour. Oscillation frequencies may be greater than the Rayleigh value, and the restoring force may be either capillary or elastic.

The characteristic equation suggests that damped viscoelastic drop oscillations may be used to determine the deformation retardation time λ_2 and the dynamic viscosity η_0 in the Jeffreys law from the measured oscillation frequency and damping rate. The accuracy of the frequency and damping rate measurement required for this purpose is below 1 %. Work is under way to establish this technique as a standard for measuring the polymeric time scale λ_2, which is to date difficult to obtain for polymer solutions.

Acknowledgements

The authors acknowledge fruitful discussions with Priv.-Doz. Dr I. Roisman from SLA at Darmstadt University of Technology in Darmstadt, Germany, who brought up the idea to determine polymer retardation times from drop oscillations.

REFERENCES

Apfel, R. E., Tian, Y. R., Jankovsky, J., Shi, T., Chen, X., Holt, R. G., Trinh, E., Croonquist, A., Thornton, K. C., Sacco, A. Jr., Coleman, C., Leslie, F. W. & Matthiesen, D. H. 1997 Free oscillations and surfactant studies of superdeformed drops in microgravity. *Phys. Rev. Lett.* **78**, 1912–1915.

Aske, N., Orr, R. & Sjöblom, J. 2002 Dilatational elasticity moduli of water–crude oil interfaces using the oscillating pendant drop. *J. Dispersion Sci. Technol.* **23**, 809–825.

Bauer, H. F. 1985 Surface and interface oscillations in an immiscible spherical visco-elastic system. *Acta Mechanica* **55**, 127–149.

BAUER, H. F. & EIDEL, W. 1987 Vibrations of a visco-elastic spherical immiscible liquid system. *Z. Angew. Math. Mech. – J. Appl. Math. Mech.* **67**, 525–535.

BIRD, R. B., ARMSTRONG, R. C. & HASSAGER, O. 1987 *Dynamics of Polymeric Liquids*. John Wiley & Sons.

BIRD, R. B., STEWART, W. E. & LIGHTFOOT, E. N. 1960 *Transport Phenomena*. John Wiley & Sons.

CHANDRASEKHAR, S. 1959 The oscillations of a viscous liquid globe. *Proc. Lond. Math. Soc.* **9**, 141–149.

DENN, M. M. 1990 Issues in viscoelastic fluid mechanics. *Annu. Rev. Fluid Mech.* **22**, 13–34.

EGRY, I., LOHÖFER, G., SEYHAN, I., SCHNEIDER, S. & FEUERBACHER, B. 1998 Viscosity of the eutectic $Pd_{78}Cu_6Si_{16}$ measured by the oscillating drop technique in microgravity. *Appl. Phys. Lett.* **73**, 462–463.

GIESEKUS, H. W. 1994 *Phänomenologische Rheologie – Eine Einführung (Phenomenological Rheology – An Introduction)*. Springer, (in German).

HILLER, W. J. & KOWALEWSKI, T. A. 1989 Surface tension measurements by the oscillating droplet method. *Physico-Chem. Hydrodyn.* **11**, 103–112.

HO-MINH, D., MAI-DUY, N. & TRAN-CONG, T. 2010 A Cartesian-grid integrated-RBF method for viscoelastic flows. *IOP Conf. Ser.: Mater. Sci. Engng* **10**, 012210.

HSU, C. J. & APFEL, R. E. 1985 A technique for measuring interfacial tension by quadrupole oscillation of drops. *J. Colloid Interface Sci.* **107**, 467–476.

HUANG, P. Y., HU, H. H. & JOSEPH, D. D. 1998 Direct simulation of the sedimentation of elliptic particles in Oldroyd-B fluids. *J. Fluid Mech.* **362**, 297–325.

JOSEPH, D. D. 1990 *Fluid Dynamics of Viscoelastic Liquids*. Springer.

KHISMATULLIN, D. B. & NADIM, A. 2001 Shape oscillations of a viscoelastic drop. *Phys. Rev.* E **63**, 061508.

KOVALCHUK, V. I., KRÄGEL, J., AKSENENKO, E. V., LOGLIO, G. & LIGGIERI, L. 2001 Oscillating bubble and drop techniques. In *Novel Methods to Study Interfacial Layers*, pp. 485–516. Elsevier.

LAMB, H. 1881 On the oscillations of a viscous spheroid. *Proc. Lond. Math. Soc.* **13**, 51–66.

LAMB, H. 1932 *Hydrodynamics*, 6th edn. Cambridge University Press.

LARSON, R. G. 1988 *Constitutive Equations for Polymer Melts and Solutions*. Butterworths.

MILLER, C. A. & SCRIVEN, L. E. 1968 The oscillations of a fluid droplet immersed in another fluid. *J. Fluid Mech.* **32**, 417–435.

PEREZ, M., SALVO, L., SUÉRY, M., BRÉCHET, Y. & PAPOULAR, M. 2000 Contactless viscosity measurement by oscillations of gas-levitated drops. *Phys. Rev.* E **61**, 2669–2675.

PHILLIPS, T. N. & WILLIAMS, A. J. 1999 Viscoelastic flow through a planar contraction using a semi-Lagrangian finite volume method. *J. Non-Newtonian Fluid Mech.* **87**, 215–246.

PROSPERETTI, A. 1980 Free oscillations of drops and bubbles: the initial-value problem. *J. Fluid Mech.* **100**, 333–347.

RAYLEIGH, LORD (J. W. STRUTT) 1879 On the capillary phenomena of jets. *Proc. R. Soc. Lond.* A **29**, 71–97.

STELTER, M., BRENN, G., YARIN, A. L., SINGH, R. P. & DURST, F. 2000 Validation and application of a novel elongational device for polymer solutions. *J. Rheol.* **44**, 595–616.

TIAN, Y. R., HOLT, R. G. & APFEL, R. E. 1995 Investigations of liquid surface rheology of surfactant solutions by droplet shape oscillations: theory. *Phys. Fluids* **7**, 2938–2949.

TRINH, E., ZWERN, A. & WANG, T. G. 1982 An experimental study of small-amplitude drop oscillations in immiscible liquid systems. *J. Fluid Mech.* **115**, 453–474.

TSAMOPOULOS, J. A. & BROWN, R. A. 1983 Nonlinear oscillations of inviscid drops and bubbles. *J. Fluid Mech.* **127**, 519–537.

YARIN, A. L., BRENN, G., KASTNER, O., RENSINK, D. & TROPEA, C. 1999 Evaporation of acoustically levitated droplets. *J. Fluid Mech.* **399**, 151–204.